Coexistence of superconductivity and magnetism in CaK(Fe_{1−x}Ni_{x})_{4}As_{4} as probed by ^{57}Fe Mössbauer spectroscopy

Sergey L. Bud'ko, Vladimir G. Kogan, Ruslan Prozorov, William R. Meier, Mingyu Xu, and Paul C. Canfield

Phys. Rev. B **98**, 144520 — Published 30 October 2018

DOI: 10.1103/PhysRevB.98.144520

Coexistence of superconductivity and magnetism in $CaK(Fe_{1-x}Ni_x)_4As_4$ as probed by ^{57}Fe Mössbauer spectroscopy

Sergey L. Bud'ko[1,2], Vladimir G. Kogan[1], Ruslan Prozorov[1,2],
William R. Meier[2], Mingyu Xu[1,2], and Paul C. Canfield[1,2]
[1]*Ames Laboratory, US DOE, Iowa State University, Ames, Iowa 50011, USA and*
[2]*Department of Physics and Astronomy,*
Iowa State University, Ames, Iowa 50011, USA

(Dated: October 12, 2018)

Abstract

Temperature dependent ^{57}Fe Mössbauer spectroscopy and specific heat measurements for $CaK(Fe_{1-x}Ni_x)_4As_4$ with $x = 0$, 0.017, 0.033, and 0.049 are presented. No magnetic hyperfine field (e.g. no static magnetic order) down to 5.5 K was detected for $x = 0$ and 0.017 in agreement with the absence of any additional feature below superconducting transition temperature, T_c, in the specific heat data. The evolution of magnetic hyperfine field with temperature was studied for $x = 0.033$ and 0.049. The long-range magnetic order in these two compounds coexists with superconductivity. The magnetic hyperfine field, B_{hf}, (ordered magnetic moment) below T_c in $CaK(Fe_{0.967}Ni_{0.033})_4As_4$ is continuously suppressed with the developing superconducting order parameter. The $B_{hf}(T)$ data for $CaK(Fe_{0.967}Ni_{0.033})_4As_4$, and $CaK(Fe_{0.951}Ni_{0.049})_4As_4$ can be described reasonably well by Machida's model for coexistence of itinerant spin density wave magnetism and superconductivity [K. Machida, J. Phys. Soc. Jpn. **50**, 2195 (1981)]. We demonstrate directly that superconductivity suppresses the spin density wave order parameter if the conditions are right, in agreement with the theoretical analysis.

PACS numbers:

I. INTRODUCTION

Co-existence and competition of superconductivity and magnetism has been of interest for condensed matter community for a long time.[1–11] Whereas in the past superconductivity and magnetism were often originating from different subsystems (e. g. with magnetism coming from local moments of rare earth, R^{3+} as in RRh_4B_4, $RMo_6(S,Se)_8$, RNi_2B_2C[2–7,7,8,8–11]), iron - based superconductors[12–16] offer the case of superconductivity and itinerant magnetism competing in the same, shared, electron subsystem. There is a commonly accepted understanding in these materials that one needs to sufficiently suppress magnetic (spin density wave) order to induce and stabilize superconductivity. The competition between superconductivity and magnetism in iron - based superconductors (in particular, in $Ba(Fe_{1-x}T_x)_2As_2$, T = Co, Ni) was observed as a reduction of the average static Fe moment below T_c inferred from the integrated intensity of the antiferromagnetic reflection in neutron scattering experiments.[17–20] ^{57}Fe Mössbauer study in another member of the 122 family, $Ba_{0.75}K_{0.25}Fe_2As_2$,[21] showed a decrease in the magnetic hyperfine field, but no change in the magnetic volume fraction below T_c, a result that was interpreted as an indication of the microscopic coexistence of magnetism and superconductivity.

Recently, several members of a new structure type in the family of iron-based superconductors, $AeAFe_4As_4$ (Ae = Ca, Sr, Eu; A = K, Rb, Cs), so-called 1144 superconductors, were discovered.[22,23] These compounds are stoichiometric superconductors and do not require tuning by substitution or pressure to exhibit superconductivity. Successful growth and basic characterization of $CaKFe_4As_4$ single crystals[24,25] opened the door for detailed studies of its superconducting and normal state properties. More importantly, it was followed by successful transition metal (Co and Ni) substitution for Fe in $CaKFe_4As_4$.[27] As a result of this substitution, a new, spin-vortex-crystal magnetic phase[26] was stabilized in $CaK(Fe_{1-x}T_x)_4As_4$ (T = Co, Ni) and range of T - concentrations where superconductivity coexists with magnetism was outlined.[27] Bulk superconductivity in these samples was suggested by magnetic and transport measurements, as well as by the size of the jump in the specific heat at T_c (see Appendix A).

Given the unusual nature of the magnetic phase, availability of homogeneous single crystals, and accessible superconducting and magnetic ordering temperatures, these materials present a fertile playground to study competition between superconductivity and magnetism

with microscopic, local probes. The elastic neutron scattering study of several of these compounds has been recently completed.[28] However, as discussed in Ref. [21], Bragg intensities reflect the product of magnetic volume fraction and magnitude of magnetic moments, whereas ^{57}Fe Mössbauer spectroscopy can address magnetic phase separation in the samples.

In this work we present temperature dependent ^{57}Fe Mössbauer spectroscopy data on $CaK(Fe_{1-x}Ni_x)_4As_4$ samples with $x = 0.017$, 0.033, and 0.049. Using these data we analyze coexistence and competition of superconductivity and magnetism in 1144 family, and refine $x - T$ phase diagram. The Mössbauer spectroscopy data will be compared with the results for pure, $x = 0$, $CaKFe_4As_4$.[29]

II. EXPERIMENTAL DETAILS

Single crystals of $CaK(Fe_{1-x}Ni_x)_4As_4$ were grown out of a high-temperature solution rich in transition-metals and arsenic similar to the procedure used for the pure compound, see Refs. [24,25,27] for further details. The Ni - composition in the samples was determined using wavelength-dispersive x-ray spectroscopy.[27] The crystals were screened[24] to avoid possible contaminations by minority phases. Mössbauer spectroscopy measurements were performed using a SEE Co. conventional, constant acceleration type spectrometer in transmission geometry with a ^{57}Co(Rh) source kept at room temperature. The absorbers were prepared as a mosaic of single crystals held on a VWR Weighting Paper disk by a small amount of Apiezon N grease. An effort was made to keep gaps between crystals to a minimum and the part of the disk not covered by crystals was coated with tungsten powder (Alfa Aesar 99.9% metals basis). The c axis of the crystals in the mosaic was parallel to the Mössbauer γ - beam. The absorber was cooled to a desired temperature using a Janis model SHI-850-5 closed cycle refrigerator (with vibration damping). The driver velocity was calibrated using an α - Fe foil, and all isomer shifts (IS) are quoted relative to the α - Fe foil at room temperature. A limited set of data for $CaK(Fe_{0.951}Ni_{0.049})_4As_4$ taken with different source and absorber was presented in Ref. [27]. The Mössbauer spectra were fitted using the commercial software package MossWinn.[30]

III. RESULTS

Subsets of Mössbauer spectra for $CaK(Fe_{1-x}Ni_x)_4As_4$ samples with $x = 0.017$, 0.033, and 0.049 are shown in Fig. 1. For $CaK(Fe_{0.983}Ni_{0.017})_4As_4$ [Fig. 1(a)] the absorption lines are asymmetric, suggesting that each spectrum is a quadrupole split doublet with rather small value of the quadrupole splitting, QS. There are no extra features observed, confirming that the samples are single phase. For the spectrum taken at the base temperature, $T = 5.5$ K, there is no apparent broadening that could be associated with a hyperfine field at the ^{57}Fe site, e.g. no evidence of a long range magnetic order, at least down to 5.5 K. All in all the Mössbauer spectra for $CaK(Fe_{0.983}Ni_{0.017})_4As_4$ are closely reminiscent of those for pure $CaKFe_4As_4$.[29]

The evolution of the spectra on cooling for two other samples, $CaK(Fe_{0.967}Ni_{0.033})_4As_4$ and $CaK(Fe_{0.951}Ni_{0.049})_4As_4$ [Figs. 1(b),(c)], is very different. At high temperatures, in the paramagnetic state, the spectra are doublets that are very similar to those of $CaKFe_4As_4$ and $CaK(Fe_{0.983}Ni_{0.017})_4As_4$. At low temperatures the spectra broaden and change their shape. These low temperature data can be fit with a magnetic sextet. The full Hamiltonian approach ("Mixed $M + Q$ Static Hamiltonian (Mosaic)" model in the MossWinn[30] software package) was used to analyze these spectra. For $T \leq 40$ K ($CaK(Fe_{0.967}Ni_{0.033})_4As_4$) and $T \leq 50$ K ($CaK(Fe_{0.951}Ni_{0.049})_4As_4$) the the fits yield the angle θ between the directions of magnetic moments and γ - rays close to 90°, suggesting that the magnetic moments are in the ab - plane, as has been argued in Ref. [27].

The temperature dependence of the hyperfine field on ^{57}Fe in $CaK(Fe_{0.967}Ni_{0.033})_4As_4$ and $CaK(Fe_{0.951}Ni_{0.049})_4As_4$ is shown in Fig. 2. For $CaK(Fe_{0.951}Ni_{0.049})_4As_4$ B_{hf} increases smoothly on cooling below $\sim$ 55 K and does not show any obvious anomaly associated with the formation of the superconducting state. For $CaK(Fe_{0.967}Ni_{0.033})_4As_4$, B_{hf} initially increases on cooling below $\sim$ 45 K, and then, on further cooling below $T_c \approx 20$ K, decreases continuously. The theoretical discussion of this behavior is presented in the next section. This behavior is comparable to that observed in Mössbauer study of $Ba_{0.75}K_{0.25}Fe_2As_2$,[21] and in elastic neutron scattering data for transition metal substituted $BaFe_2As_2$,[17–20] and recently $CaK(Fe_{1-x}Ni_x)_4As_4$.[28]

Temperature and Ni-concentration dependences of the isomer shift and quadrupole splitting are presented in Appendix B. Comparison of the temperature dependent, ^{57}Fe hyperfine

field with the temperature dependence of the ordered moment inferred from elastic neutron scattering is presented in Appendix C.

IV. DISCUSSION

A. Suppression of magnetic order by the emerging superconducting state

The problem of superconductivity coexisting with charge density wave order has been considered by Bilbro and McMillan within a weak-coupling BCS model for both order parameters.[31] K. Machida applied the same formalism to the question of coexistence of superconductivity and spin density wave.[32] The model was developed for an anisotropic, three-dimensional, single band case, yet it captures the main experimental features.The superconducting critical temperature, in absence of magnetism, is given by $\Delta_0(0)/k_BT_{c0} = \pi/e^C \approx 1.76$ ($C \approx 0.577$ is the Euler constant, $\Delta_0(0)$ is the gap at $T = 0$.). Similarly, for the pure magnetic order parameter we have $M_0(0)/k_BT_{s0} = \pi/e^C \approx 1.76$; here M_0 is the energy gap in the electron spectrum over the salient part of the Fermi surface in the absence of superconducting order and the transition temperature for the magnetic transition is $T_{s0} > T_{c0}$. The spin density wave (SDW) order is assumed to develop over a nested part of the Fermi surface with the relative density of states $N_1/N_0 = n_1 < 1$, whereas the superconductivity forms over, and gaps the full Fermi surface with the DOS N_0 without SDW, and part of the DOS, $N_2 = N_0 - N_1$ when SDW is present. When both orders coexist, the order parameters $M(T)$ and $\Delta(T)$ satisfy the system of two coupled self-consistency equations[32]:

$$\ln\frac{T}{T_{s0}} = 2\pi T\sum_{\omega>0}^{\omega_s}\left[\frac{1}{2M}\left(\frac{M+\Delta}{\sqrt{\omega^2+(M+\Delta)^2}}+\frac{M-\Delta}{\sqrt{\omega^2+(M-\Delta)^2}}\right)-\frac{1}{\omega}\right], \quad (1)$$

$$\ln\frac{T}{T_{c0}} = n_1 2\pi T\sum_{\omega>0}^{\omega_D}\left[\frac{1}{2\Delta}\left(\frac{\Delta+M}{\sqrt{\omega^2+(\Delta+M)^2}}+\frac{\Delta-M}{\sqrt{\omega^2+(\Delta-M)^2}}\right)-\frac{1}{\omega}\right] + n_2 2\pi T\sum_{\omega}^{\omega_D}\left(\frac{1}{\sqrt{\omega^2+\Delta^2}}-\frac{1}{\omega}\right). \quad (2)$$

Here, $\omega = \pi T(2n+1)$ are Matsubara frequencies with integer $n \geq 0$, ω_D is the Debye frequency, ω_s is a corresponding limit for SDW, and $n_2 = 1 - n_1$. For brevity we use units with Plank's $\hbar$ and Boltzmann's k_B as unities, so that temperature and frequency have units of energy. The sums here are convergent and for $\omega_D \gg T_{c0}$ and $\omega_s \gg T_{s0}$ the upper limits of summation can be extended to infinity.

For numerical work aimed at the situation with $T_{s0} > T_{c0}$, it is convenient to introduce dimensionless variables

$$t = \frac{T}{T_{s0}}\,, \quad d = \frac{\Delta}{2\pi T_{s0}}\,, \quad m = \frac{M}{2\pi T_{s0}}\,. \tag{3}$$

After some rearrangements, Eqs. (1), (2) take the form:

$$m \ln t = \sum_{n\geq 0}^{\infty} \left[\frac{t}{2} \left(\frac{m+d}{\sqrt{t^2(n+1/2)^2 + (m+d)^2}} + \frac{m-d}{\sqrt{t^2(n+1/2)^2 + (m-d)^2}} \right) - \frac{m}{n+1/2} \right], \tag{4}$$

$$d \ln(Rt) = n_1 \sum_{n\geq 0}^{\infty} \left[\frac{t}{2} \left(\frac{d+m}{\sqrt{t^2(n+1/2)^2 + (m+d)^2}} + \frac{d-m}{\sqrt{t^2(n+1/2)^2 + (d-m)^2}} \right) - \frac{d}{n+1/2} \right]$$
$$+ n_2 d \sum_{n\geq 0}^{\infty} \left(\frac{t}{\sqrt{t^2(n+1/2)^2 + d^2}} - \frac{1}{n+1/2} \right), \tag{5}$$

where $R = T_{s0}/T_{c0} > 1$. Fig.3 shows numerical solutions for $n_1 = 0.05$ and $n_1 = 0.3$, $R = T_{s0}/T_{c0} = 2$ and $R = 4$. Clearly, the SDW order parameter at $T_c < T < T_{s0}$ has a standard BCS temperature dependence.

Fig. 3 shows that the effect of superconductivity on the magnetic order parameter is larger for smaller values of n_1, e.g. for smaller nesting (for constant R), and for smaller R (for constant n_1). Qualitatively, and expectedly, it means that (within the model) magnetism is more robust than superconductivity. To observe measurable suppression of magnetic order parameter below T_c one has to have small nesting and/or not very different bare T_{s0} and T_{c0} values. Fig. 3 also shows that one can have similar behavior of m and d as a function of temperature for different values of R and n_1. As such, a unique determination R and n_1 would require additional boundary conditions on them.

To obtain an equation for T_c, the superconducting transition temperature in the presence of magnetic order, one multiplies Eq. (5) by d and goes to the limit $d \to 0$:

$$\ln(Rt_c) = n_1 \sum_{n>0}^{\infty} \left(\frac{(n+1/2)^2}{[(n+1/2)^2 + m_c^2/t_c^2]^{3/2}} - \frac{1}{n+1/2} \right), \tag{6}$$

where $t_c = T_c/T_{s0}$ and m_c is the normalized magnetization at t_c. This equation contains two unknowns, t_c and m_c. Since $d = 0$ at t_c, the magnetization satisfies the equation for $m_c(t_c)$:

$$\ln t_c = \sum_{n>0}^{\infty} \left(\frac{1}{\sqrt{(n+1/2)^2 + m_c^2/t_c^2}} - \frac{1}{n+1/2} \right). \tag{7}$$

In other words, for given R and n_1, the system of Eqs. (6) and (7) can be solved for t_c and m_c. The result is shown in Fig. 4 for $R = 2$; in particular, it shows that the superconductivity is practically suppressed for $n_1 > 0.8$. Grossly speaking, Fig. 4 is an illustration of the fact that both the SDW and superconductivity are built from gapping Fermi surface; if there is almost no Fermi surface left for superconductivity, then t_c drops toward zero.

Figure 2 shows that the experimental data for the two samples of $CaK(Fe_{1-x}Ni_x)_4As_4$ (magnetic hyperfine field serves as a proxy for magnetization) can be fit quite well by Machida's model. As discussed above, this is not necessarily a unique fit, and additional analysis and experimental data are required to justify these particular values of model parameters. It is important to stress that our measurements provide direct access to magnetic order parameter magnitude, not just usually measured transition temperature. Thus we demonstrate directly that superconductivity does suppress the spin density wave order, in agreement with the theoretical analysis.

B. Magnetic hyperfine field, Néel temperature and x - T phase diagram

Analysis of the experimental data of magnetic hyperfine field and the magnetic ordering temperature (see e.g. Ref. [33]) suggested proportionality between B_{hf} at base temperature and T_N that translates into $T_N \propto M$, where M is the Fe effective moment. For $CaK(Fe_{0.951}Ni_{0.049})_4As_4$ superconductivity has no apparent effect on $B_{hf}(T)$ (Fig. 2). To evaluate the hyperfine field at base temperature in absence of superconductivity for For $CaK(Fe_{0.967}Ni_{0.033})_4As_4$ we use the results of fits in Fig. 2.

The plot of B_{hf} vs T_N for these two compounds together with the literature data for several members of 122 and 1111 families is shown in Fig. 5. Although, for the two 1144 compounds studied here, the difference between the values of T_N and the inferred values of B_{hf} is rather small, it appears that the gross trend of $B_{hf} \propto T_N$ observed in 122 family probably holds for 1144, although studies on larger set of samples are required to support (or refute) this statement.

Finally, the thermodynamic, specific heat (Appendix A), and spectroscopic, Mössbauer, measurements allow us to confirm and refine the $x - T$ phase diagram for $CaK(Fe_{1-x}Ni_x)_4As_4$.[27] Both experimental techniques used in this work allow for the detection of magnetic ordering above, as well as below, the superconducting transition. For

the $x = 0.017$ sample there is no broadening of the Mössbauer spectra at low temperatures, that could be associated with a static magnetic hyperfine field on the ^{57}Fe site and no additional anomalies in $C_p(T)$ below T_c. Consequently no long range magnetic order exists for $CaK(Fe_{0.983}Ni_{0.017})_4As_4$, at least above either 5.5 K ($B_{hf} = 0$) or 1.9 K ($C_p(T)$). The current suggested $x-T$ phase diagram is shown in Fig. 6. This phase diagram is consistent with the rather general, simple model in Ref. [32] that predicts that the magnetic spin density wave state is precluded when the superconductivity develops at a higher temperature, since the superconducting energy gap opens all over the Fermi surface and prohibits the formation of the spin density wave gap. On the other hand, when the onset temperature of the spin density wave is higher than that of superconductivity, these two long range orders, according to Ref. [32] generally coexist. It is noteworthy that recent theoretical work on coexistence of superconductivity and magnetism in iron pnictides[42] suggested similar $x-T$ phase diagram for the case of $s^{\pm}$ superconducting pairing. Further studies for $0.017 < x < 0.033$ will be needed to determine fine details of whether there is "back-bending" of the T_N line once T_N drops below T_c.

V. SUMMARY

Our ^{57}Fe Mössbauer study of $CaK(Fe_{1-x}Ni_x)_4As_4$ compounds detected no magnetic hyperfine field (e.g. no static magnetic order) down to 5.5 K for $x = 0.017$ and followed the evolution of B_{hf} with temperature for $x = 0.033$ and 0.049. The long-range magnetic spin-vortex-crystal order[27] was found to coexist with superconductivity, however, similar to the doped 122 compounds, the magnetic hyperfine field (ordered magnetic moment) below T_c in $CaK(Fe_{0.967}Ni_{0.033})_4As_4$ is continuously suppressed with the developing superconducting order parameter. The $B_{hf}(T)$ data for $CaK(Fe_{0.967}Ni_{0.033})_4As_4$, and $CaK(Fe_{0.951}Ni_{0.049})_4As_4$ were analyzed using the model of Machida for coexistence of itinerant spin density wave magnetism and superconductivity.[32] It is remarkable that this rather simple model can account for experimental observations in real, complex materials.

Similarly to 122 compounds, the values of T_N and base temperature B_{hf} are roughly proportional, suggesting that the value of T_N in the $CaK(Fe_{1-x}Ni_x)_4As_4$ family is mainly affected by the value of the magnetic moment on iron.

In addition, specific heat data on $CaK(Fe_{1-x}Ni_x)_4As_4$ (Appendix A) allowed for additional

thermodynamically determined points on the $x-T$ phase diagram as well as additional values of ΔC_p at T_c which were found to follow BNC scaling.[43]

The isomer shift was found to have insignificant Ni-concentration dependence, whereas both quadrupole splitting and line width monotonically increase with Ni concentration.

Acknowledgments

Work at the Ames Laboratory was supported by the U.S. Department of Energy, Office of Science, Basic Energy Sciences, Materials Sciences and Engineering Division. The Ames Laboratory is operated for the U.S. Department of Energy by Iowa State University under contract No. DE-AC02-07CH11358. WRM was supported by the Gordon and Betty Moore Foundation's EPiQS Initiative through Grant GBMF4411.

Appendix A: Specific heat

In addition to electrical resistivity and magnetic susceptibility measurements[24,27] on the $CaK(Fe_{1-x}Ni_x)_4As_4$ samples with x =0, 0.017, 0.033, and 0.049, the temperature dependent specific heat measurements, using a hybrid adiabatic relaxation technique of the heat capacity option in a Quantum Design, Physical Property Measurement System instrument were performed on these samples. The data, plotted as C_p/T vs T are shown in Fig. 7

The data clearly show the evolution of the superconducting and magnetic transitions with Ni- substitution. T_c decreases with Ni-doping, in agreement with the published phase diagram[27] as does the jump in the specific heat at T_c. The signatures corresponding to the magnetic phase transitions are observed only for $x = 0.033$, 0.049, with no anomaly below T_c found for $x = 0$ or $x = 0.017$. Altogether the specific heat data allows to confirm and refine, with a thermodynamic measurement, the $x-T$ phase diagram for $CaK(Fe_{1-x}Ni_x)_4As_4$ suggested in Ref. [27].

It has been shown[43–47] that for many iron-based superconductors, in particular of 122 family, an empirical trend, so called BNC scaling, $\Delta C_p|_{T_c} \propto T_c^3$ is observed. Moreover, deviation from such scaling was suggested to be a signature of significant changes in the nature of the superconducting state.[46,48,49] The data for $CaK(Fe_{1-x}Ni_x)_4As_4$ (x =0, 0.017, 0.033, and 0.049) were added to the BNC plot (Fig. 8) (to be consistent with the previous data for

the 122 family, for this plot the molecular weight was taken as 1/2 of the molecular weight of $CaK(Fe_{1-x}Ni_x)_4As_4$). These data agree well with the rough, $\Delta C_p|_{T_c} \propto T_c^3$ trend, suggesting that the nature of superconductivity is probably similar to that in the majority of the members of the 122 family. At the same time there data are consistent with superconductivity in $CaK(Fe_{1-x}Ni_x)_4As_4$ being bulk.

Appendix B: Hyperfine parameters

Isomer shift and quadrupole splitting as a function of temperature are plotted for $CaK(Fe_{1-x}Ni_x)_4As_4$, $x = 0$, 0.017, 0.033, and 0.049 in Fig. 9. Taken together, all data are very consistent. In the paramagnetic state the isomer shift for all four compounds is almost the same (it decreases by $\sim 2\%$ between $x = 0$ and $x = 0.049$, Fig. 10). This means that the changes in the local electron density at the iron site, as well as the difference in the Debye temperatures that dominate the $IS(T)$ dependence, are insignificant (cf. small $< 4\%$ changes in the IS values in the $(Ba_{1-x}K_x)(Fe_{1-y}Co_y)_2As_2$[33]). The quadrupole splitting increases with Ni - substitution (Fig. 10). This could be related to the change of local environment of the ^{57}Fe accompanying change of the lattice parameters (see Ref. [27], Supplemental Information), however further structural work as well as band structure calculations would be required to understand this trend.

For $CaK(Fe_{1-x}Ni_x)_4As_4$, $x = 0.033$, and 0.049 there is minor change in the isomer shift values between paramagnetic and the magnetically ordered state. The increase of IS by $\sim 5\%$ suggests that the local electron density at the iron site increases in the magnetically ordered state. Some changes of electronic structure in the ordered state are expected, since the magnetic unit cell doubles in in the spin-vortex-crystal state. ARPES experiments are desirable for understanding of these changes. The is no apparent change in the $|QS|$ at the transition within the scattering of the results.

Appendix C: Comparison with neutron scattering data

Temperature dependent, hyperfine field data for $CaK(Fe_{0.967}Ni_{0.033})_4As_4$, and $CaK(Fe_{0.951}Ni_{0.049})_4As_4$ are plotted in Fig. 11 together with the square root of the intensity measured at the (1/2 1/2 3) antiferromagnetic Bragg peak position for both samples that

is proportional to the antiferromagnetic moment, the antiferromagnetic order parameter.[28] These two sets of data scale fairly well, with scaling coefficient being different by $\sim 12\%$ between $x = 0.033$ and 0.049 data sets. This comparison of two data sets, obtained on the samples grown in very similar way, give confidence in use of Mössbauer spectroscopy for further studies of coexistence of superconductivity and magnetism in iron-based superconductors. In addition, this comparison allows for the evaluation of the ratio between the magnetic hyperfine field and the magnetic moment (A) in the 1144 materials.[50] Taking two values of the magnetic moment cited in Ref. [28] and comparing them with the corresponding values of B_{hf} yields $A \approx 6.3$ T/μ_B. This value is the same as repoted for $BaFe_2As_2$[34,51].

---

[1] M. Brian Maple, Appl. Phys. **9**, 179 (1976).

[2] K. N. Shrivastava, K. P. Sinha, Phys. Repts **115**, 93 (1984).

[3] A. I. Buzdin, L. N. Bulaevskii, M. L. Kulich, and S. V. Panyukov, Usp. Fiz. Nauk **144**, 597 (1984) [Sov. Phys. Usp. **27**, 927 (1984)].

[4] A. I. Buzdin, L. N. Bulaevskii, Usp. Fiz. Nauk **149**, 45 (1986) [Sov. Phys. Usp. **29**, 412 (1986)].

[5] S. L. Kakani and U. N. Upadhyaya, J. Low Temp. Phys **70**, 5 (1988).

[6] Ø. Fischer in: Ferromagnetic Materials v.5 (North-Holland, Amsterdam, 1990) Edited by K. H. J. Buschow and E. P. Wohlfarth, p.465.

[7] Paul C. Canfield, Peter L. Gammel, and David J. Bishop, Physics Today **51** (10), 40 (1998).

[8] K.-H. Müller and V. N. Narozhnyi, Rep. Prog. Phys. **64**, 943 (2001).

[9] Comptes Rendus Physique, **7**, 1 (2006), Special Issue "Superconductivity and magnetism", Edited by A. Buzdin.

[10] P. Carretta, R. De Renzi, G. Prando, and S. Sanna, Phys. Scr. **88**, 068504 (2013).

[11] C. T. Wolowiec, B. D. White, and M. B. Maple, Physica C **514**, 113 (2015).

[12] David C. Johnston, Adv. Phys. **59**, 803 (2010).

[13] Paul C. Canfield and Sergey L. Bud'ko, Ann. Rev. Cond. Mat. Phys. **1**, 27 (2010).

[14] G. R. Stewart, Rev. Mod. Phys. **83** 1589 (2011).

[15] Andrey Chubukov, and Peter J. Hirschfeld, Physics Today **68** (6), 46 (2015).

[16] Comptes Rendus Physique, **17**, 1 (2016), Special Issue "Iron-based Superconductors", Edited by H. Alloul and A. Cano.

[17] D. K. Pratt, W. Tian, A. Kreyssig, J. L. Zarestky, S. Nandi, N. Ni, S. L. Bud'ko, P. C. Canfield, A. I. Goldman, and R. J. McQueeney, Phys. Rev. Lett. **103**, 087001 (2009).

[18] A. D. Christianson, M. D. Lumsden, S. E. Nagler, G. J. MacDougall, M. A. McGuire, A. S. Sefat, R. Jin, B. C. Sales, and D. Mandrus, Phys. Rev. Lett. **103**, 087002 (2009).

[19] M. Wang, H. Luo, J. Zhao, C. Zhang, M. Wang, K. Marty, S. Chi, J. W. Lynn, A. Schneidewind, S. Li, and P. Dai, Phys. Rev. B **81**, 174524 (2010).

[20] Huiqian Luo, Rui Zhang, Mark Laver, Zahra Yamani, Meng Wang, Xingye Lu, Miaoyin Wang, Yanchao Chen, Shiliang Li, Sung Chang, Jeffrey W. Lynn, and Pengcheng Dai, Phys. Rev. Lett. **108**, 247002 (2012).

[21] J. Munevar, H. Micklitz, J. Agüero, Guotai Tan, Chenglin Zhang, Pengcheng Dai, and E. Baggio-Saitovitch, Phys. Rev. B **88**, 184514 (2013).

[22] Akira Iyo, Kenji Kawashima, Tatsuya Kinjo, Taichiro Nishio, Shigeyuki Ishida, Hiroshi Fujihisa, Yoshito Gotoh, Kunihiro Kihou, Hiroshi Eisaki, and Yoshiyuki Yoshida, J. Am. Chem. Soc. **138**, 3410 (2016).

[23] Yi Liu, Ya-Bin Liu, Zhang-Tu Tang, Hao Jiang, Zhi-Cheng Wang, Abduweli Ablimit, Wen-He Jiao, Qian Tao, Chun-Mu Feng, Zhu-An Xu, and Guang-Han Cao, Phys. Rev. B **93**, 214503 (2016).

[24] W. R. Meier, T. Kong, U. S. Kaluarachchi, V. Taufour, N. H. Jo, G. Drachuck, A. E. Böhmer, S. M. Saunders, A. Sapkota, A. Kreyssig, M. A. Tanatar, R. Prozorov, A. I. Goldman, Fedor F. Balakirev, Alex Gurevich, S. L. Bud'ko, and P. C. Canfield, Phys. Rev. B **94**, 064501 (2016).

[25] W. R. Meier, T. Kong, S. L. Bud'ko, and P. C. Canfield, Phys. Rev. Materials **1**, 013401 (2017).

[26] Joseph O'Halloran, D. F. Agterberg, M. X. Chen, and M. Weinert, Phys. Rev. B **95**, 075104 (2017).

[27] William R. Meier, Qing-Ping Ding, Andreas Kreyssig, Sergey L. Bud'ko, Aashish Sapkota, Karunakar Kothapalli, Vladislav Borisov, Roser Valentí, Cristian D. Batista, Peter P. Orth, Rafael M. Fernandes, Alan I. Goldman, Yuji Furukawa, Anna E. Böhmer, and Paul C. Canfield, npj Quant. Mater. **3**, 5 (2018).

[28] A. Kreyssig, J. M. Wilde, A. E. Böhmer, W. Tian, W. R. Meier, Bing Li, B. G. Ueland, Mingyu Xu, S. L. Bud'ko, P. C. Canfield, R. J. McQueeney, and A. I. Goldman, Phys. Rev. B **97**, 224521 (2018).

[29] Sergey L. Bud'ko, Tai Kong, William R. Meier, Xiaoming Ma, and Paul C. Canfield, Philos.

Mag. **97**, 2689 (2017).

[30] Zoltán Klencár, MossWinn 4.0 Manual (2016).

[31] G. Bilbro and W. L. McMillan, Phys. Rev. B **14**, 1887 (1976).

[32] K. Machida, J. Phys. Soc. Jpn. **50**, 2195 (1981).

[33] Til Goltz, Veronika Zinth, Dirk Johrendt, Helge Rosner, Gwendolyne Pascua, Hubertus Luetkens, Philipp Materne, and Hans-Henning Klauss, Phys. Rev. B **89**, 144511 (2014).

[34] Marianne Rotter, Marcus Tegel, Dirk Johrendt, Inga Schellenberg, Wilfried Hermes, and Rainer Pöttgen, Phys. Rev. B **78**, 020503 (2008).

[35] Marianne Rotter, Marcus Tegel, Inga Schellenberg, Falko M. Schappacher, Rainer Pöttgen, Joachim Deisenhofer, Axel Günther, Florian Schrettle, Alois Loidl and Dirk Johrendt, New J. Phys. **11**, 025014 (2009).

[36] Marcus Tegel, Marianne Rotter, Veronika Weiß, Falko M. Schappacher, Rainer Pöttgen, and Dirk Johrendt, J. Phys.: Cond. Mat. **20**, 452201 (2008).

[37] M. Alzamora, J. Munevar, E Baggio-Saitovitch, S. L. Bud'ko, Ni Ni, P. C. Canfield, and D R Sánchez, J. Phys.: Cond. Mat. **23**, 145701 (2011).

[38] Israel Nowik, Israel Felner, V. P. S. Awana, Arpita Vajpayee, and H. Kishan, J. Phys.: Cond. Mat. **20**, 292201 (2008).

[39] H.-H. Klauss, H. Luetkens, R. Klingeler, C. Hess, F. J. Litterst, M. Kraken, M. M. Korshunov, I. Eremin, S.-L. Drechsler, R. Khasanov, A. Amato, J. Hamann-Borrero, N. Leps, A. Kondrat, G. Behr, J. Werner, and B. Büchner, Phys. Rev. Lett. **101**, 077005 (2008).

[40] Michael A. McGuire, Andrew D. Christianson, Athena S. Sefat, Brian C. Sales, Mark D. Lumsden, Rongying Jin, E. Andrew Payzant, David Mandrus, Yanbing Luan, Veerle Keppens, Vijayalaksmi Varadarajan, Joseph W. Brill, Raphaël P. Hermann, Moulay T. Sougrati, Fernande Grandjean, and Gary J. Long, Phys. Rev. B **78**, 094517 2008.

[41] M. Tegel, S. Johansson, V. Weiß, I. Schellenberg, W. Hermes, R. Pöttgen and D. Johrendt, EPL **84**, 67007 (2008).

[42] Rafael M. Fernandes and Jörg Schmalian, Phys. Rev. B **82**, 014521 (2010)

[43] S. L. Bud'ko, N. Ni, and P. C. Canfield, Phys. Rev. B **79**, 220516 (2009).

[44] J. S. Kim, G. R. Stewart, S. Kasahara, T. Shibauchi, T. Terashima, and Y. Matsuda, J. Phys.: Condens. Matter **23**, 222201 (2011).

[45] J. S. Kim, B. D. Faeth, and G. R. Stewart, Phys. Rev. B **86**, 054509 (2012).

[46] Sergey L. Bud'ko, Mod. Phys. Lett. B **29**, 1430019 (2015).

[47] Yunkyu Bang and G R Stewart, J. Phys.: Condens. Matter **29**, 123003 (2017).

[48] Sergey L. Bud'ko, Mihai Sturza, Duck Young Chung, Mercouri G. Kanatzidis, and Paul C. Canfield, Phys. Rev. B **87**, 100509 (2013).

[49] V. Grinenko, D. V. Efremov, S.-L. Drechsler, S. Aswartham, D. Gruner, M. Roslova, I. Morozov, K. Nenkov, S. Wurmehl, A. U. B. Wolter, B. Holzapfel, and B. Büchner, Phys. Rev. B **89**, 060504 (2014).

[50] S. M. Dubiel, J. Alloys Compd. **488**, 18 (2009).

[51] Q. Huang, Y. Qiu, Wei Bao, M. A. Green, J. W. Lynn, Y. C. Gasparovic, T. Wu, G. Wu, and X. H. Chen, Phys. Rev. Lett. **101**, 257003 (2008).

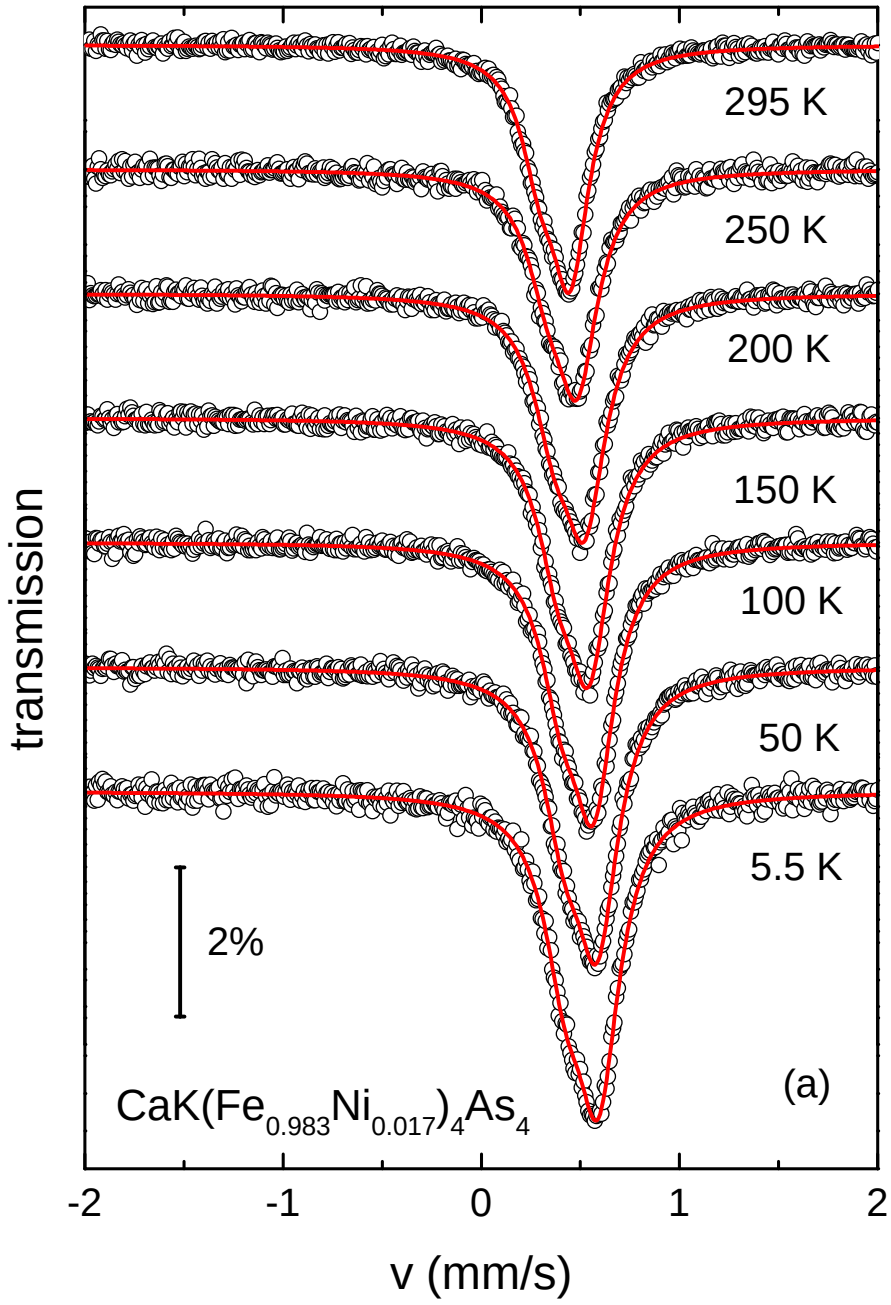
295 K
250 K
200 K
150 K
100 K
50 K
5.5 K
2%
(a)
CaK(Fe0.983Ni0.017)4As4
transmission
-2
-1
0
1
2
v (mm/s)

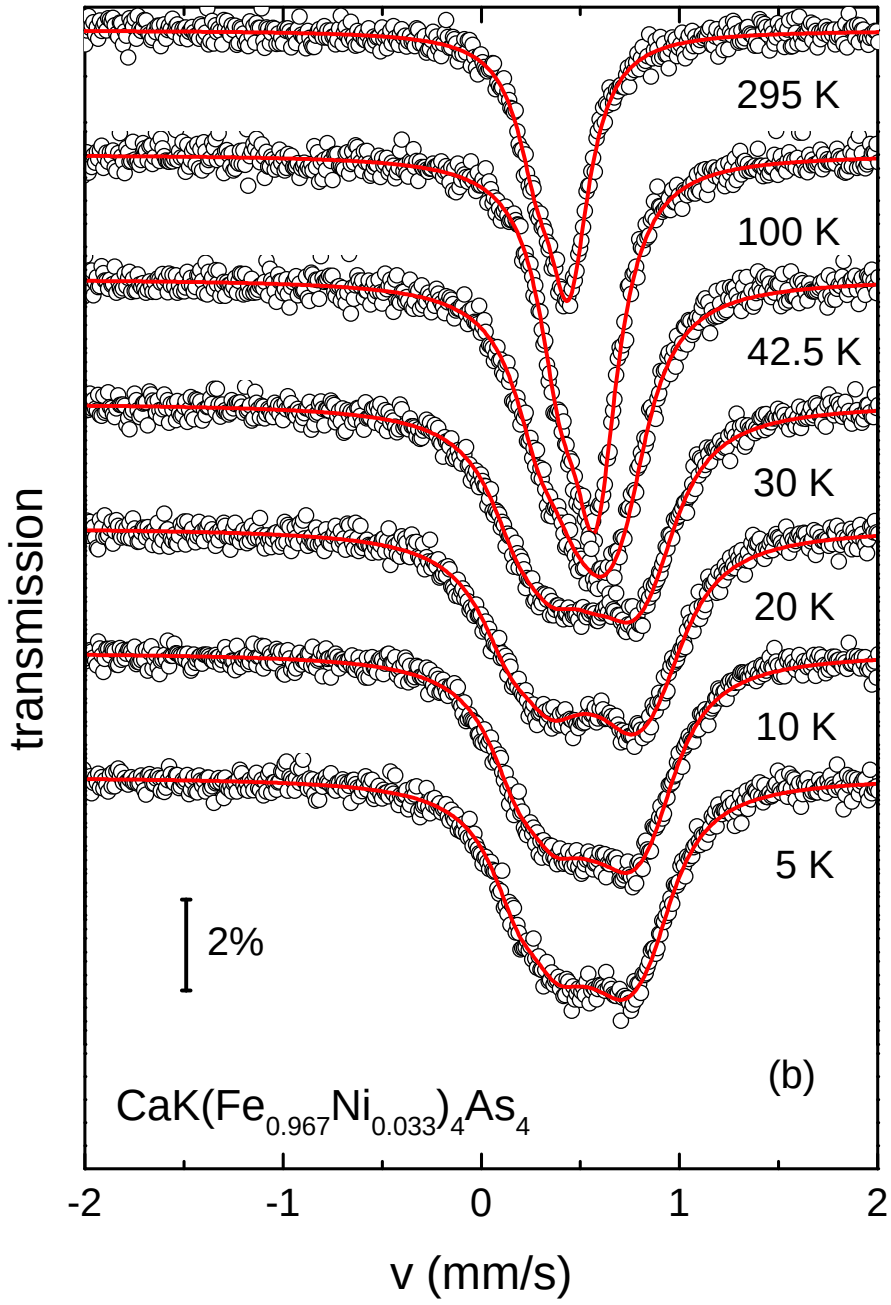
295 K
100 K
42.5 K
30 K
20 K
10 K
5 K
2%
(b)
CaK(Fe0.967Ni0.033)4As4
transmission
-2
-1
0
1
2
v (mm/s)

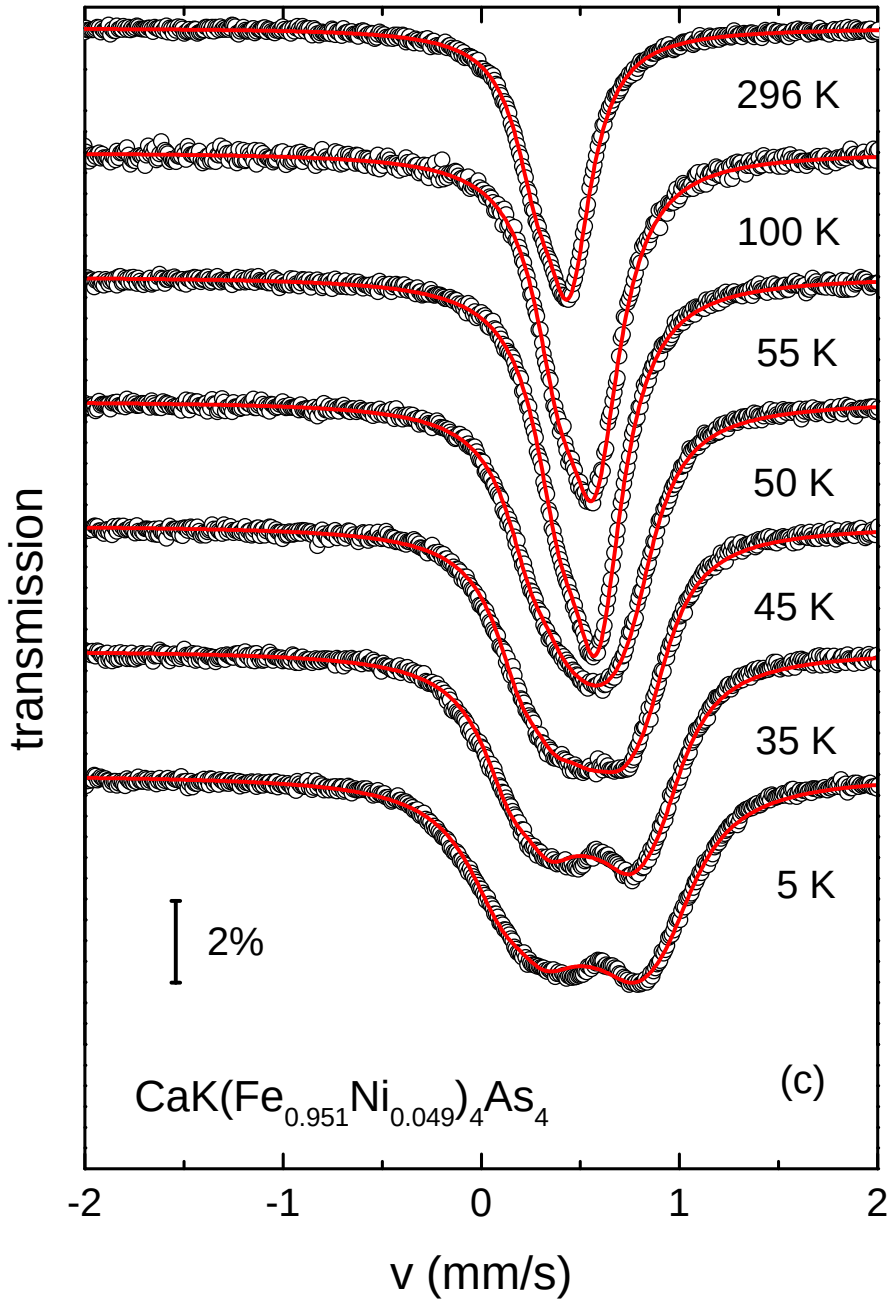

FIG. 1: (color online) ^{57}Fe Mössbauer spectra of (a) $CaK(Fe_{0.983}Ni_{0.017})_4As_4$, (b) $CaK(Fe_{0.967}Ni_{0.033})_4As_4$, and (c) $CaK(Fe_{0.951}Ni_{0.049})_4As_4$, at selected temperatures. Symbols - data, lines - fits.

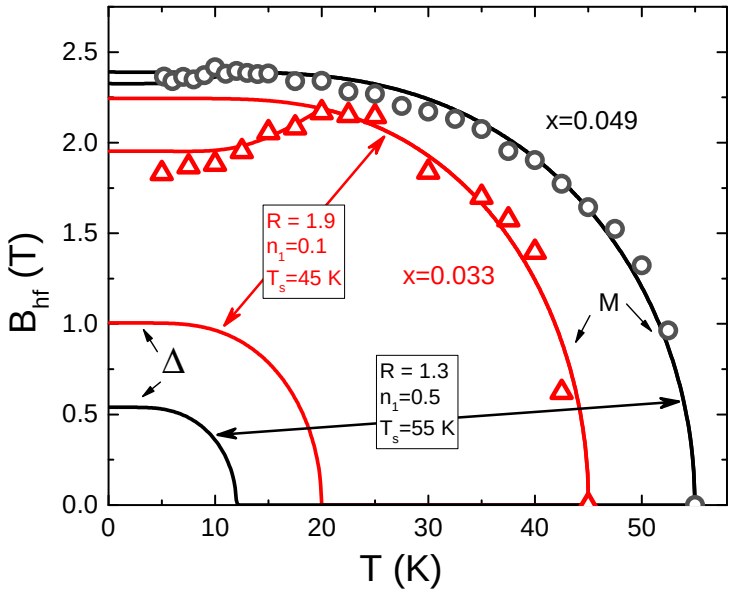

FIG. 2: (Color online) Experimental data (symbols) of $B_{hf}(T)$ for $CaK(Fe_{0.967}Ni_{0.033})_4As_4$, and $CaK(Fe_{0.951}Ni_{0.049})_4As_4$ overlayed with temperature dependence of scaled magnetic, M, and superconducting, Δ order parameters (lines) from fits using model of Ref. [32] (with $B_{hf}(T)$ serving as a proxy for magnetization). Obtained fitting parameters are listed on the plot.

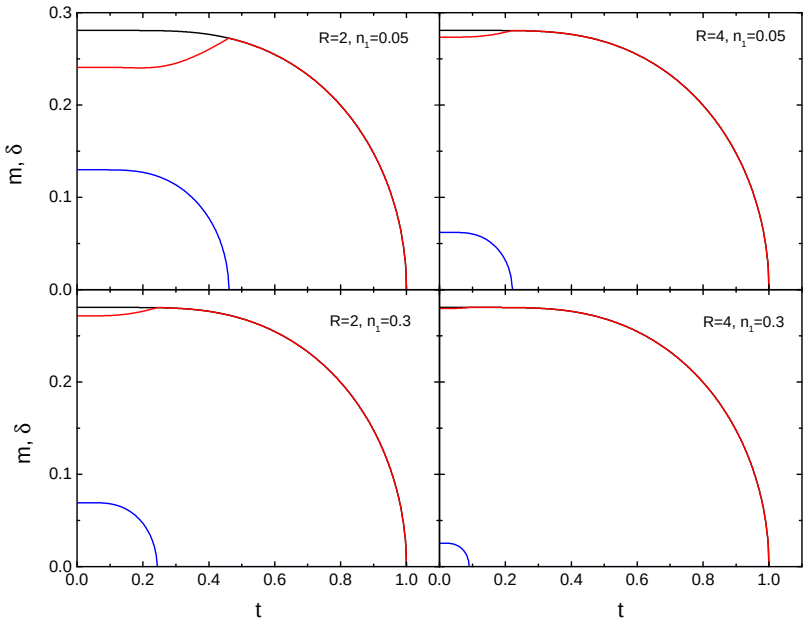

FIG. 3: (Color online) Magnetic (red line) and superconducting (blue line) order parameters for $R = T_{s0}/T_{c0} = 2$ and $R = 4$. The black line is for part of "bare" $m_0(t)$ below T_c. (See text for details)

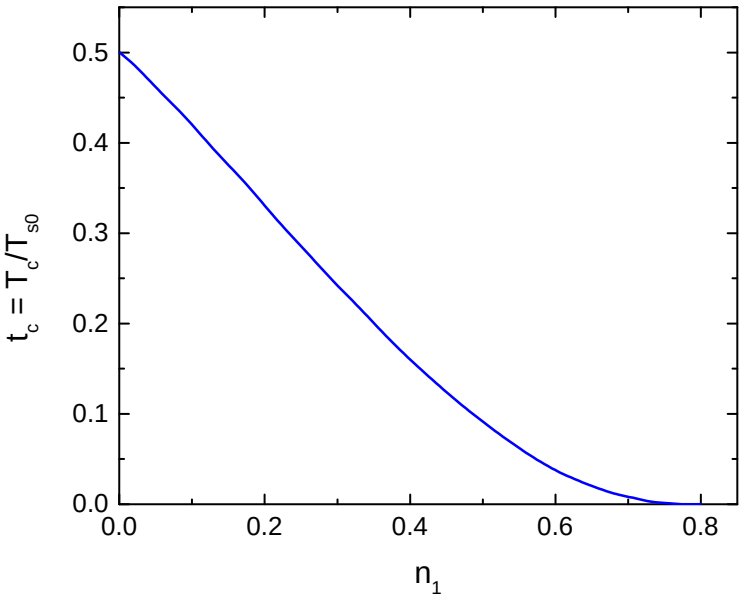

FIG. 4: (Color online) $t_c = T_c/T_{s0}$ as a function of n_1 for $R = 2$.

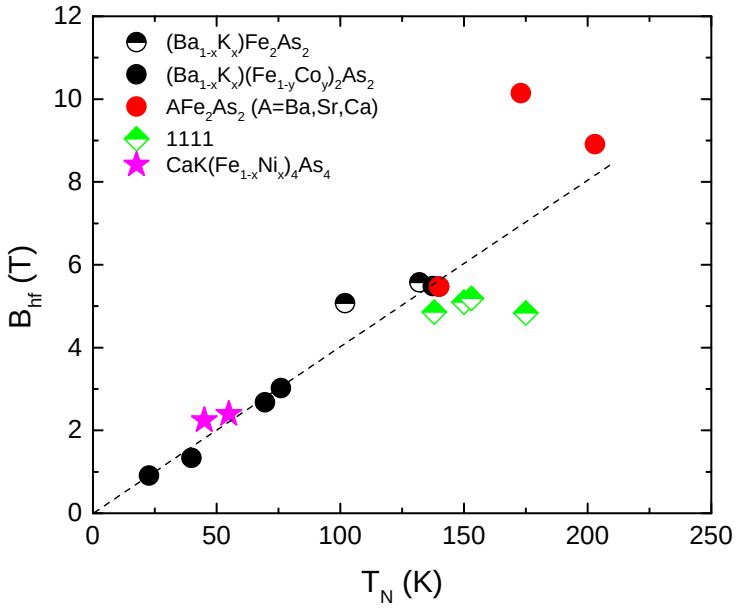

FIG. 5: (color online) The value of magnetic hyperfine field on ^{57}Fe sites as a function of the Néel temperature for several Fe-based superconductors and related materials. Data for $CaK(Fe_{1-x}Ni_x)_4As_4$ - this work, other points are taken from the literature.[33–41] Dashed line - linear fit for $(Ba_{1-x}K_x)(Fe_{1-y}Co_y)_2As_2$.[33]

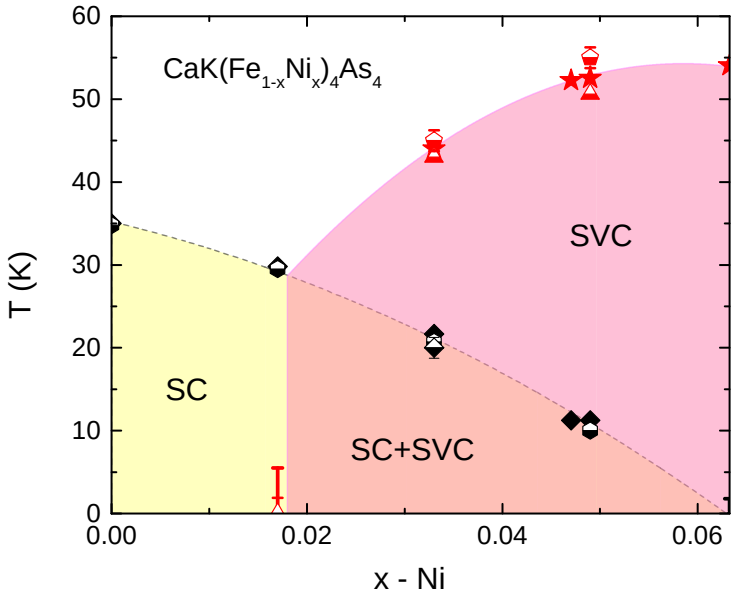

FIG. 6: (color online) $x-T$ phase diagram for $CaK(Fe_{1-x}Ni_x)_4As_4$. Phases: SC - superconducting; SVC - magnetic spin vortex crystal, SC+SVC - coexistence of superconductivity and spin vortex crystal magnetic order. Symbols: filled - from Ref. [27], half - filled - this work: triangles and hexagons - from $C_p(T)$, pentagons and rhombus - from Mössbauer spectroscopy. Lines are guides for the eye.

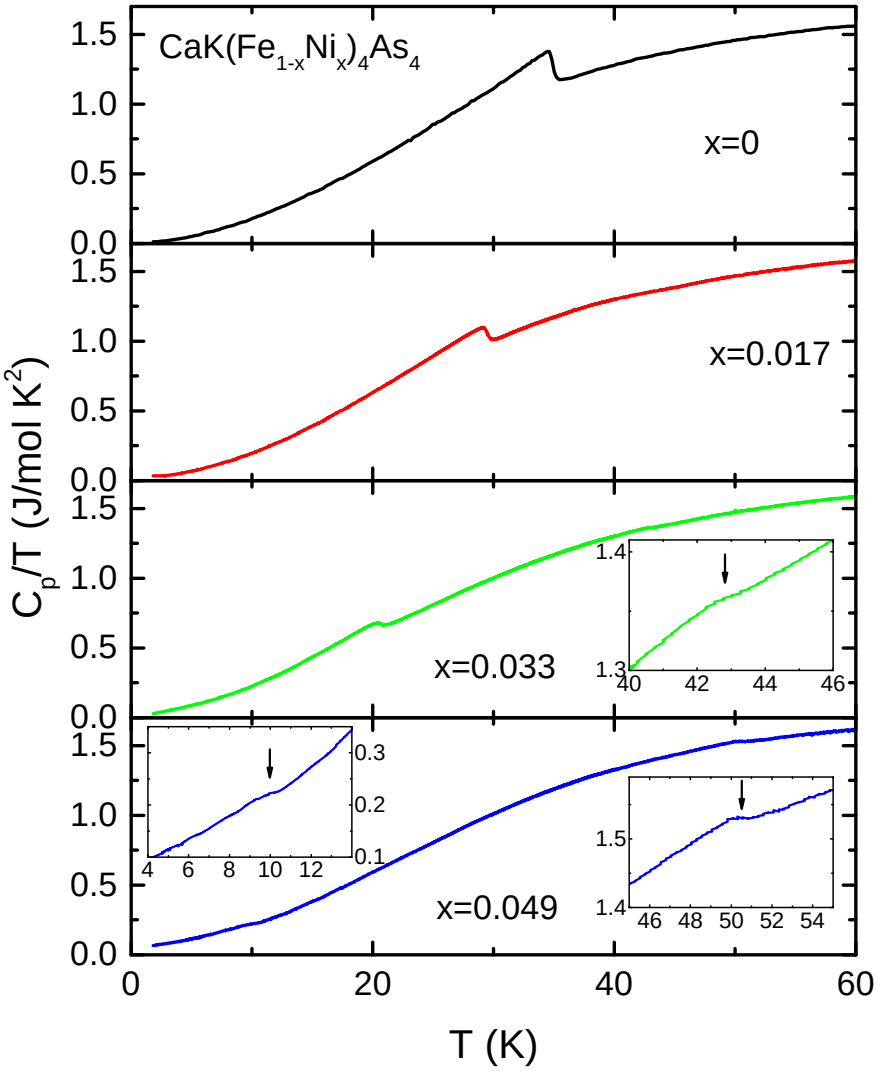

FIG. 7: (color online) Temperature dependent specific heat of $CaK(Fe_{1-x}Ni_x)_4As_4$ samples with x = 0, 0.017, 0.033, and 0.049 plotted as C_p/T vs T. Insets - enlarged parts of the plots at magnetic (x = 0.033, 0.049 panels, right) and superconducting (x = 0.49 panel, left) transitions. Arrows in the insets mark the transition temperatures. Some of the data were previously shown in Refs. [24,27].

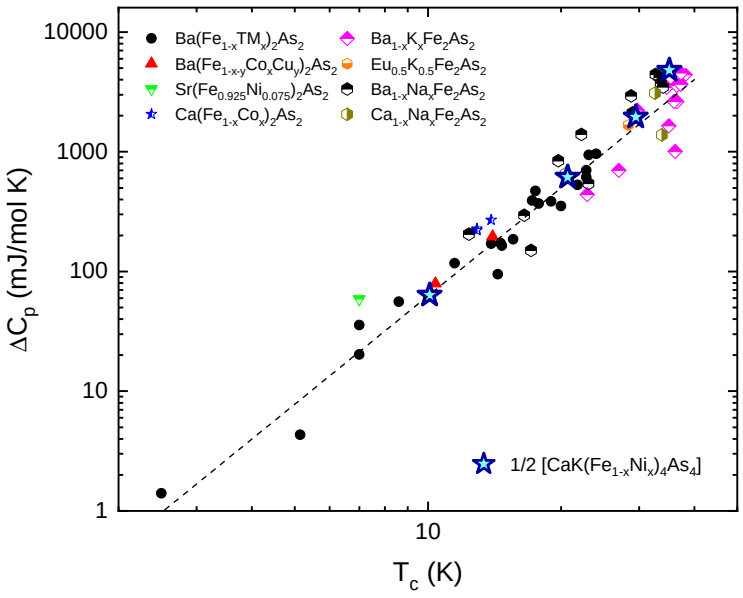

FIG. 8: (color online) ΔC_p at the superconducting transition vs T_c for the $CaK(Fe_{1-x}Ni_x)_4As_4$ samples with $x = 0$, 0.017, 0.033, and 0.049 plotted together with literature data[46] for various Fe-based superconductors. For consistency, half of the molecular weight of 1144 samples was taken for this plot. Literature data for KFe_2As_2 and close concentrations[46] are not shown for simplicity.

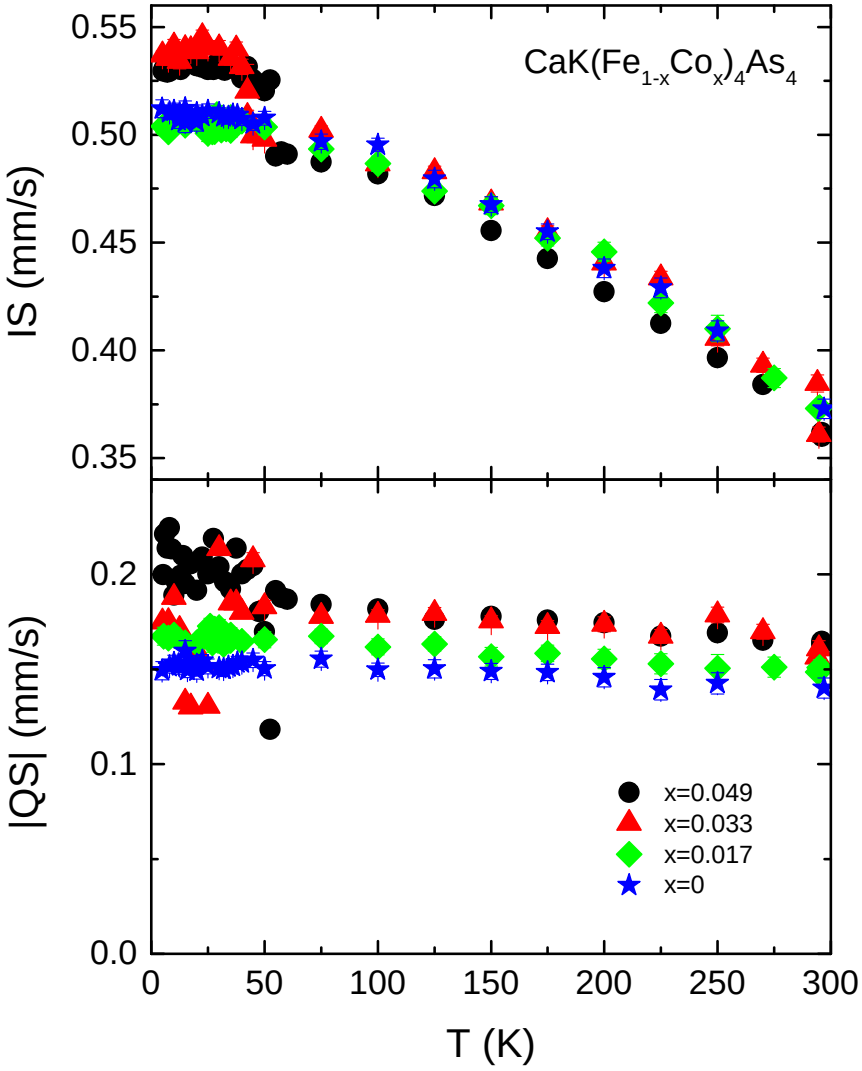

FIG. 9: (color online) Temperature dependent hyperfine parameters obtained from fits of ^{57}Fe Mössbauer spectra of $CaK(Fe_{1-x}Ni_x)_4As_4$ samples with $x = 0$, 0.017, 0.033, and 0.049. at different temperatures: (a) isomer shift (IS), (b) absolute value of the quadrupole splitting (|QS|). Data for $CaKFe_4As_4$ are taken from Ref. [29].

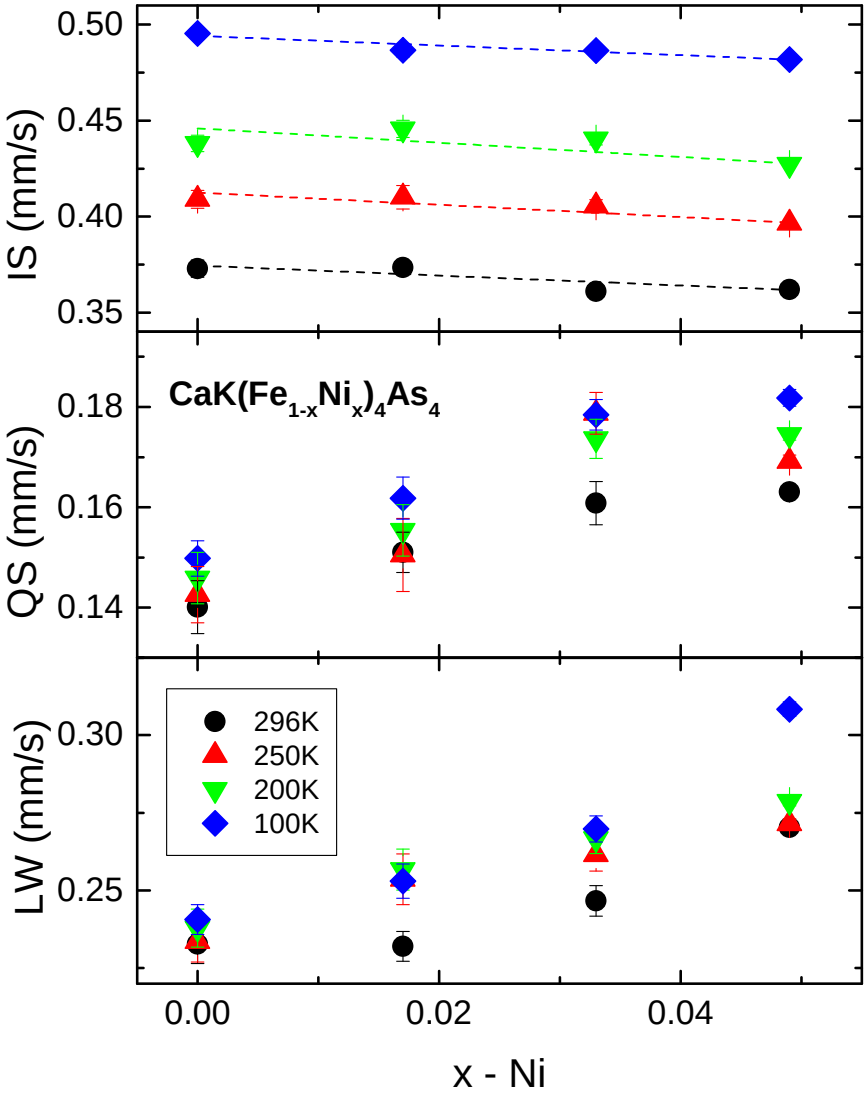

FIG. 10: (color online) Hyperfine parameters, isomer shift, (b) quadrupole splitting, and line width at selected temperatures, obtained from fits of ^{57}Fe Mössbauer spectra of $CaK(Fe_{1-x}Ni_x)_4As_4$ samples with $x = 0$, 0.017, 0.033, and 0.049, plotted as a function of Ni - concentration, x. Data for $CaKFe_4As_4$ are taken from Ref. [29]. Dashed lines - linear fits.

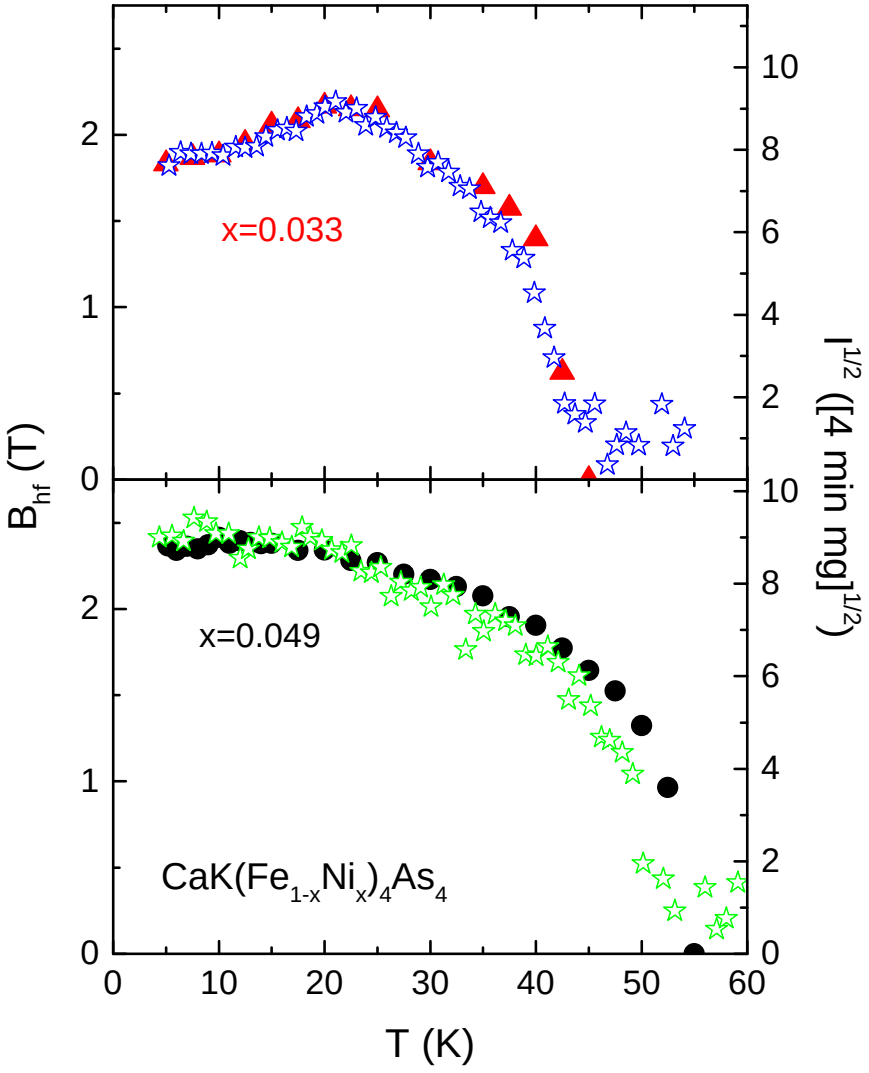

FIG. 11: (color online) Temperature dependent hyperfine field (filled and half-filled symbols, left axes) of $CaK(Fe_{1-x}Ni_x)_4As_4$ samples with $x = 0.033$, and 0.049, plotted together with the square root of the intensity of the (1/2 1/2 3) antiferromagnetic Bragg peak from neutron scattering data in Ref. [28] (open symbols, right axes).